



Brain endothelial STING1 activation by *Plasmodium*-sequestered heme promotes cerebral malaria via type I IFN response

Teresa F. Pais^{a,1} , Hajrabibi Ali^a , Joana Moreira da Silva^{a,b}, Nádia Duarte^a , Rita Neres^a , Chintan Chhatbar^{c,d} , Rita C. Acúrcio^e , Rita C. Guedes^e, Maria Carolina Strano Moraes^f, Bruno Costa-Silva^f, Ulrich Kalinke^g, and Carlos Penha-Gonçalves^{a,1}

Edited by L. Sibley, Washington University in St. Louis, St. Louis, MO; received April 13, 2022; accepted August 4, 2022

Cerebral malaria (CM) is a life-threatening form of *Plasmodium falciparum* infection caused by brain inflammation. Brain endothelium dysfunction is a hallmark of CM pathology, which is also associated with the activation of the type I interferon (IFN) inflammatory pathway. The molecular triggers and sensors eliciting brain type I IFN cellular responses during CM remain largely unknown. We herein identified the stimulator of interferon response cGAMP interactor 1 (STING1) as the key innate immune sensor that induces *Irf1* transcription in the brain of mice infected with *Plasmodium berghei* ANKA (*Pba*). This STING1/IFN β -mediated response increases brain CXCL10 governing the extent of brain leukocyte infiltration and blood–brain barrier (BBB) breakdown, and determining CM lethality. The critical role of brain endothelial cells (BECs) in fueling type I IFN–driven brain inflammation was demonstrated in brain endothelial–specific IFN β -reporter and STING1-deficient *Pba*-infected mice, which were significantly protected from CM lethality. Moreover, extracellular particles (EPs) released from *Pba*-infected erythrocytes activated the STING1-dependent type I IFN response in BECs, a response requiring intracellular acidification. Fractionation of the EPs enabled us to identify a defined fraction carrying hemoglobin degradation remnants that activates STING1/IFN β in the brain endothelium, a process correlated with heme content. Notably, stimulation of STING1-deficient BECs with heme, docking experiments, and in vitro binding assays unveiled that heme is a putative STING1 ligand. This work shows that heme resultant from the parasite heterotrophic activity operates as an alarmin, triggering brain endothelial inflammatory responses via the STING1/IFN β /CXCL10 axis crucial to CM pathogenesis and lethality.

STING1 | IFN beta | cerebral malaria | brain endothelium | CXCL10

Malaria, the disease caused by *Plasmodium* infection, accounted for over 400,000 deaths worldwide in 2019 (World Malaria Report 2019). Despite the available malarial treatments, children under 5 y of age can develop cerebral malaria (CM) upon infection with *Plasmodium falciparum*, facing the highest risk of severe malaria morbidity and mortality (15 to 20%) (1). Brain swelling with increased compression of respiration centers in the brainstem predicts a fatal CM outcome (2). Children who survive CM are often affected by long-term neurological sequelae (1).

Infected erythrocytes (IEs), parasite components released during the blood-stage infection (e.g., malarial hemozoin and labile heme), and systemic inflammatory factors (e.g., CXCL10, TNF, IL1 β , and IFN γ) elicit an unfettered brain endothelial cell response that compromises regular endothelium function (reviewed in ref. 3). In particular, blood–brain barrier (BBB) integrity is lost, which results in leakage of plasma proteins and water into the cerebral parenchyma and consequent intracranial hypertension (reviewed in ref. 4). However, whether brain endothelial cells (BECs) are bystander activated by systemic inflammatory factors or the actual source of brain inflammation and pathology remains largely unexplored in CM.

Over the last years, the type I interferons, IFN α and IFN β , emerged as key mediators in innate immune responses to malaria, promoting brain immunopathology (reviewed in ref. 5). In children with uncomplicated malaria, activation of the type I IFN response was associated with protective immunity (6). However, in children with CM, polymorphism in regulatory regions of type I IFN receptor (IFNAR1 subunit) gene were associated with increased type I IFN signaling and CM development (7). In the experimental mouse model of CM, despite the protective role of type I IFN in early infection (8, 9), several reports show that ablation of IFNAR1 signaling prevents BBB disruption and pathogenesis of experimental CM driven by parasite-specific cytotoxic CD8⁺ T cells (10, 11). In addition, mice deficient in type I IFN signaling

Significance

CM results from loss of blood–brain endothelial barrier function caused by unrestrained inflammatory response in the natural course of infection by *Plasmodium* parasites. However, the role of brain endothelium in triggering inflammatory mechanisms is still undetermined. We found that the innate immune sensor STING1 is crucial for production of IFN β by brain endothelial cells in *Plasmodium*-infected mice. This in turn stimulates CXCL10-mediated recruitment of leukocytes and subsequent brain inflammation and tissue damage. We identified within extracellular particles released from *Plasmodium*-infected erythrocytes, a fraction containing products of hemoglobin degradation, namely, heme, which we show can bind STING1. Our results unravel a mechanism of CM immunopathogenesis: Heme contained in extracellular particles triggers the STING1/IFN β /CXCL10 axis in brain endothelial cells.

Author contributions: T.F.P., R.C.G., and C.P.-G. designed research; T.F.P., H.A., J.M.d.S., N.D., R.N., R.C.A., and R.C.G. performed research; C.C., M.C.S.M., B.C.-S., and U.K. contributed new reagents/analytic tools; T.F.P., H.A., J.M.d.S., N.D., R.N., R.C.A., R.C.G., M.C.S.M., and C.P.-G. analyzed data; and T.F.P., N.D., and C.P.-G. wrote the paper.

The authors declare no competing interest.

This article is a PNAS Direct Submission.

Copyright © 2022 the Author(s). Published by PNAS. This article is distributed under Creative Commons Attribution-NonCommercial-NoDerivatives License 4.0 (CC BY-NC-ND).

¹To whom correspondence may be addressed. Email: mtpais@igc.gulbenkian.pt or cpenha@igc.gulbenkian.pt.

This article contains supporting information online at <http://www.pnas.org/lookup/suppl/doi:10.1073/pnas.2206327119/-/DCSupplemental>.

Published August 29, 2022.

molecules—like transcription factors interferon regulatory factor 3 (IRF3) and 7 (IRF7) and the upstream TAK-binding kinase 1 (TBK1)—show a lower degree of brain pathology with less infiltration by parasite-specific CD8⁺ T cells (11) and partial (11) or total protection from CM (12). Moreover, a point mutation in the ubiquitin-specific protease 15 (USP15) deters the type I IFN response in the mouse brain, which dampens brain inflammation and increases survival of CM (13).

Several pattern recognition receptors (PRRs) underlie inflammatory responses during *Plasmodium* infection by binding to *Plasmodium*-derived components (14), such as glycosylphosphatidylinositol (GPI) anchors, plasmodial DNA and RNA, and hemozoin—a byproduct of hemoglobin digested by the parasite, consisting of crystals made of polymerized heme (15). Labile heme, a byproduct of hemolysis during *Plasmodium* infection, can also signal via PRRs (16) and contribute to the pathogenesis of CM (17, 18).

The cGAS–STING1 pathway is a major sensor of cytosolic DNA that can recognize AT-rich motifs in plasmodial DNA and induce IFN β transcription in human monocytes and mouse macrophages (12, 19, 20). Interestingly, extracellular vesicles derived from *Plasmodium*-IEs (19) and complexes of plasmodial DNA with hemozoin (12) were proposed as carriers of parasite DNA into the cytosol of human monocytes.

BECs can also capture and cross-present malarial antigens to parasite-specific CD8⁺ T cells (21). Two mechanisms by which malarial antigens could reach the endothelial cell endosomal and cytosolic compartments were proposed, one through membrane fusion with infected erythrocytes, and another by uptake of merozoites and digestive vacuoles (21, 22).

Ubiquitous expression of type I IFN and IFNAR1 poses a significant challenge to the identification of specific cellular and molecular contributors to type I IFN signaling activation in CM development. Although BECs are within the first cells to sense the

IEs, their role in type I IFN-mediated innate immune responses during CM remains elusive. Here, we demonstrate that in the brain, specifically in BECs, STING1 activation by parasite-sequestered heme, present in particles released from *Plasmodium* IEs, is a critical mechanism underlying CM pathogenesis.

Results

Brain IFN β Production via STING1 Activation Correlates with CM.

There is indirect evidence connecting brain type I IFN responses with tissue pathology associated with CM in *Plasmodium berghei* ANKA (*Pba*)-infected mice (23). We used an IFN β -luciferase reporter mouse line (24) to directly test whether IFN β induction in the brain was triggered by *Pba* infection. We detected strong luminescence (SI Appendix, Fig. S1A) and significantly increased luciferase activity in brain tissue as well as in the lung of mice developing CM (Fig. 1A). In contrast, mice infected with *PbNK65*, a parasite strain that does not cause CM, induced weak or no luminescence signal (SI Appendix, Fig. S1B). The IFN β induction in the brain correlated with a type I response spread in three main brain regions—olfactory bulb, cerebrum, and cerebellum—as indicated by the expression of four type I IFN response interferon-stimulated genes (*Irf1*, *Irf7*, *Ift1*, and *Cxcl10*) (SI Appendix, Fig. S1C). We then assessed the contribution of IFN β to CM pathogenesis. BBB integrity was measured by Evans Blue (EB) quantification in the brain after perfusion at day 6 postinfection (PI). BBB leakage of EB was lower in the brains of IFN β knockout (KO) than in the brains of wild-type (WT) mice (Fig. 1B and SI Appendix, Fig. S1D). Accordingly, CM was less lethal in IFN β KO mice than in WT controls (Fig. 1D). This decrease in lethality was not attributable to differences in parasite burden in the blood and in the brain of IFN β KO compared to WT mice and was not affected by sex (SI Appendix, Fig. S1 E and F).

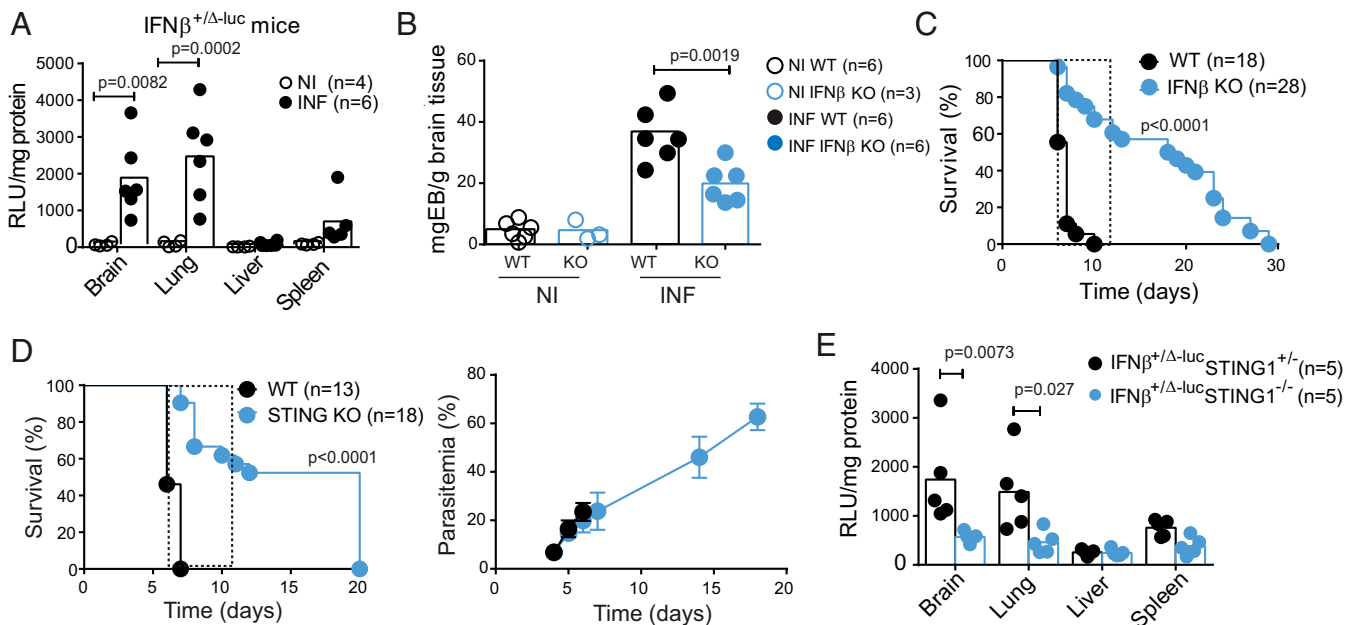


Fig. 1. Cerebral malaria pathogenesis is associated with type I IFN responses induced by STING1 activation in *Plasmodium* infection. (A) *Ifnβ1* gene expression in the indicated organs of IFN β -Luc reporter (IFN $\beta^{+/Δ-luc}$) mice infected with *Pba* (day 6 PI) or noninfected was ascertained by ex vivo luciferase activity normalized for tissue protein contents. The present data are representative of three independent experiments. (B) Blood-brain barrier integrity was evaluated by EB quantification in the brain after mouse perfusion. Data were normalized for brain weight in WT and IFN β KO mice at day 6 PI. (C) Survival curve of WT and IFN β KO mice infected with 10^6 *Pba* IE. (D) Survival and blood parasitemia curves in mice deficient for STING1. (E) Induction of *Ifnβ1* gene expression in the indicated organs of IFN β -Luc reporter (IFN $\beta^{+/Δ-luc}$ STING1^{+/-}) and in IFN β -Luc reporter lacking STING1 (IFN $\beta^{+/Δ-luc}$ STING1^{-/-}) mice infected with *Pba* (day 6 PI) was ascertained by ex vivo luciferase activity normalized for tissue protein amounts. Dashed line in C and D delimits the time window of death by CM. Data points in A, B, and E represent individual mice. Data in A, B, and E are analyzed by one-way ANOVA, Tukey's multiple comparisons test. Data in C and D comprise two independent infection experiments and are compared between mouse strains with a Gehan–Breslow–Wilcoxon test.

Several PRRs sense *Plasmodium* infection and initiate downstream signaling converging at the phosphorylation and activation of the type I interferon regulatory family of transcription factors (IRFs) (14). *Pba* IE, *Plasmodium* AT-rich DNA motifs, and parasite DNA in EPs that are released from *P. falciparum* IE were shown to activate the STING1 pathway of type I IFN induction in mouse macrophages and human monocytes in culture (12, 19). However, the role of STING1 activation in the development of CM has not been addressed. We found that *Sting1* deletion significantly delayed death by CM and conferred ~50% protection against CM lethality without affecting the parasitemia (Fig. 1D) or brain parasite load (*SI Appendix, Fig. S1F*). Although we cannot exclude minor contributions of the other PRRs, we did not detect a significant difference in CM lethality when STING1 KO mice were compared with quadruple KO mice for *Myd88*, *Trif*, *Mavs*, and *Sting1* (MyTrMaSt KO), which are impaired in all known type I response induction pathways (*SI Appendix, Fig. S1G*). Lower levels of IFN β induction, measured by luciferase activity, were also found in the brains and lungs of IFN β -reporter mice deficient for STING1 with CM (Fig. 1E). These results indicate that STING1 is a major innate immune sensor of *Pba* infection ensuing IFN β production in the brain and subsequent BBB disruption and CM development.

STING1 Activation Induces *Cxcl10* Gene Expression and Leukocyte Recruitment to the Brain. In *Pba*-infected mice, brain innate immune responses occur before leukocyte recruitment to this organ (13, 25). We used IFN β -reporter mice in both alleles to measure induction of type I IFN at early stages of infection. We detected a significant increase of luciferase activity in the brain of mice as early as day 4 PI (Fig. 2A). Next, we tested whether IFN β induction by STING1 in the brain could drive expression of *Cxcl10*, a known mediator of leukocyte recruitment downstream of IFN signaling. Deletion of *Ifn β 1* or *Sting1* significantly decreased the levels of *Cxcl10* mRNA in the brain, at day 4 PI (Fig. 2B).

Plasmodium infection induces CXCL10 in the brain, which in turn recruits CXCR3- expressing antigen-specific pathogenic CD8⁺ T cells (26–28). We analyzed whether brain leukocyte infiltration was impaired in IFN β KO and STING1 KO mice and found lower percentage (Fig. 2C) and numbers of leukocytes (CD45^{high}), namely CD8⁺ T cells (CD45⁺TCR β ⁺CD8⁺) and monocytes (CD45^{high} Mac-1⁺), in the brains of STING1 KO mice (Fig. 2D) and of IFN β KO mice (*SI Appendix, Fig. S2A*) than in those of WT mice. However, the expression of CD8⁺ T cell surface activation markers (CD44^{high}/CD62L^{low}) and of Granzyme B and IFN γ was similar in WT, STING1 KO (Fig. 2D) and IFN β KO mice (*SI Appendix, Fig. S2A*), which indicates that CD8⁺ T cell activation was equally effective. The low numbers of CD8⁺ T cells in the brain of infected STING1 KO mice could not be attributed to decreased local proliferation (25) as the frequency of BrdU⁺ cells among CD8⁺ T cells was not significantly different between WT and STING1 KO mice (*SI Appendix, Fig. S2B*). Likewise, microglia activation assessed by MHC class I (25) expression was similar in WT and KO mice (Fig. 2D and *SI Appendix, Fig. S2A*).

Notably, the decrease in the number of brain-infiltrating leukocytes was not related to a decrease in the activation of splenic T cells or monocytes in STING1 KO or IFN β KO mice (*SI Appendix, Fig. S2C*). This suggests that innate immune activation of STING1 leading to IFN β production and *Cxcl10* gene up-regulation in the brain contributes to leukocyte recruitment into the brain and immunopathology in CM.

STING1 Activation and IFN β Production by Brain Endothelial Cells Contributes to CM. It is unclear whether specific brain cell types are responsible for the induction of IFN β response to blood-borne parasites. We investigated IFN β production in different brain cells during CM by using cell type-specific IFN β -reporter mice (IFN β ^{lox/lox}-luc/lox^{lox}-luc mice bred to mice with Cre expression driven by cell-type specific promoters) (29). In these mice one *Ifn β 1* allele is kept wild-type while the other allele drives luciferase activity by the *Ifn β 1* floxed allele in cells that undergo Cre recombination. We found no significant induction of luciferase activity in astrocytes (GFAPCre⁺ mice) upon CM induction while a clear response was obtained 24 h after Poly I:C injection (Fig. 3A). On the other hand, LysMCre⁺ brain cells, including different types of myeloid cells (25), showed *Ifn β 1* transcription activation upon infection as detected by increased luciferase activity in the brain (Fig. 3B).

To determine whether IFN β is induced in microglia, the brain resident macrophage population, during CM, we used CX3CR1CreERT2^{+/−} mice (30). After Cre induction with tamoxifen, the monocyte compartment will be replenished with bone-marrow derived cells without flox excision, while the self-renewing microglia will maintain the *Ifn β 1*-luc reporter gene active and give a luciferase signal if triggered. Under these conditions, we detected luciferase activity indicating *Ifn β 1* gene transcription in the microglial cell compartment during CM (Fig. 3C).

Induction of *Ifn β 1* in the endothelial compartment was assessed in reporter mice expressing Cre in endothelial and hematopoietic cells under the Tie2 promoter (Fig. 3D), and in reporter mice carrying inducible Cre under the *Slco1c1* promoter activated specifically in brain endothelial/ependymal cells (31) (Fig. 3E). Induction of luciferase activity in both mouse lines showed that brain endothelial cells contribute to local brain production of IFN β in the brain during CM.

To determine the impact of cell-specific expression of STING1 or IFN β in CM development, we specifically deleted these genes in different cell types by using cell-lineage specific Cre expression in mice carrying two floxed alleles or one inactivated allele and one floxed allele for the target gene. We found that absence of STING1 or IFN β in LysM⁺ or CX3CR1⁺ cells did not prevent death by CM (Fig. 3F and *SI Appendix, Fig. S3A*). In contrast, ablation of STING1 or IFN β in endothelial and hematopoietic cells in mice expressing Cre under Tie2 promoter (Fig. 3G and *SI Appendix, Fig. S3B*) or ablation of STING1 specifically in brain endothelial cells in *Slco1c1*CreERT2^{+/−} mice significantly protected from CM lethality (Fig. 3H). In addition health/neurologic score on day 6 PI was improved (*SI Appendix, Fig. S3C*) while parasitemia was unaffected (*SI Appendix, Fig. S3D*). Furthermore, mice with Tie2⁺-induced STING1 deletion that survived CM showed clinical improvement after day 8 PI (*SI Appendix, Fig. S3E*) which was not attributable to decreased blood parasitemia in this time period (*SI Appendix, Fig. S3F*).

Overall, these results unveil that STING1-dependent activation of IFN β production in brain endothelial cells starting early in infection is a critical determinant of brain immunopathology during CM development.

IE-Derived EPs Induce IFN β via STING1 After Intracellular Acidification in Brain Endothelial Cells. The generation of extracellular particles (EPs) (100 to 1,000 nm) by erythrocytes has been associated with the pathogenesis of human and rodent CM (32, 33). Also, vesicles released from *P. falciparum* IE activate expression of proinflammatory cytokines (i.e., TNF and IFN β) in innate immune cells (19, 34). We asked whether EPs

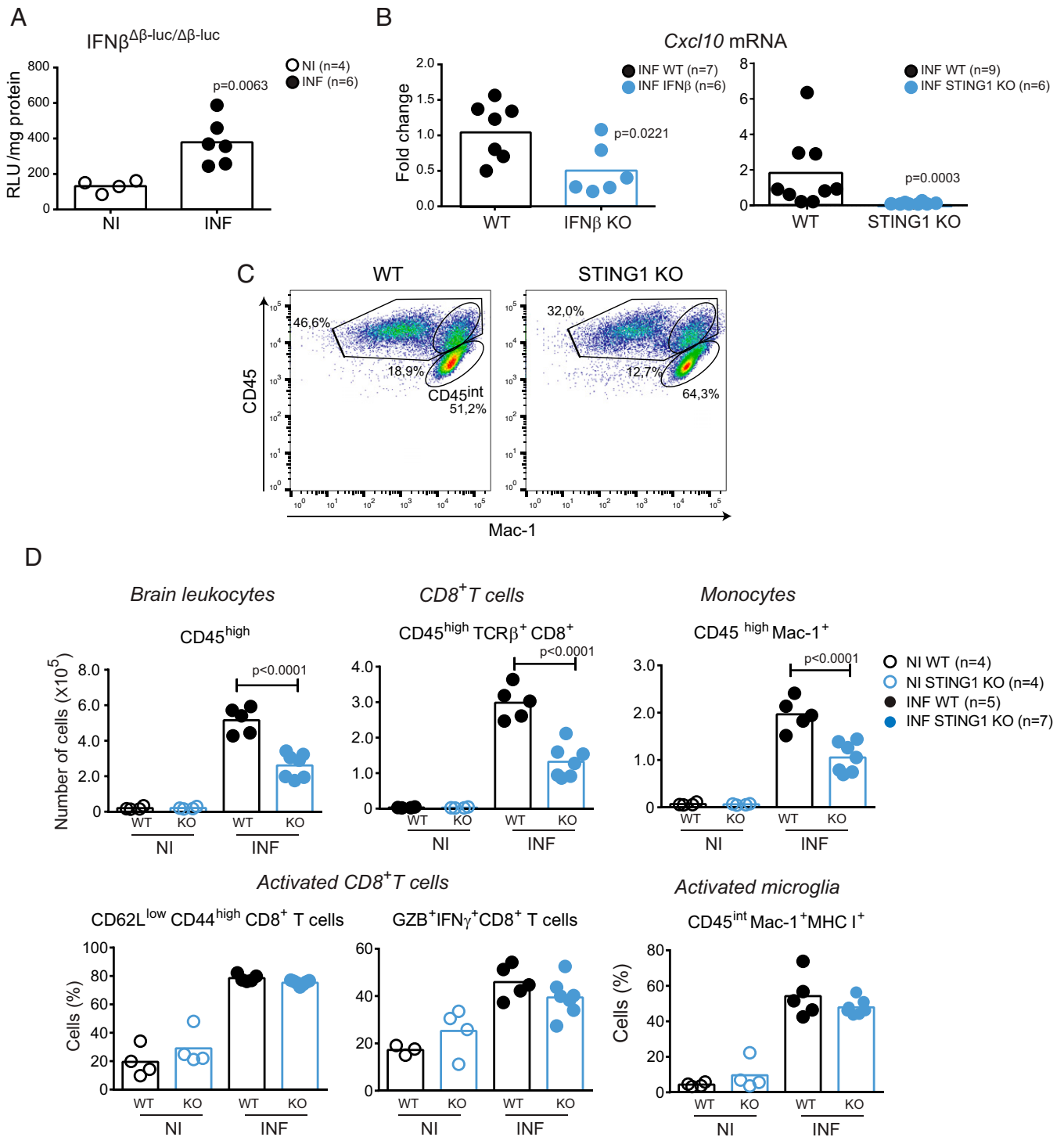


Fig. 2. Leukocyte brain infiltration is mediated by STING1 induction of *Ifnβ* and *Cxcl10* in the brain. (A) *Ifnβ1* gene expression in the brain of mice with two reporter alleles for *Ifnβ1* ($IFN\beta^{\Delta\beta-luc/\Delta\beta-luc}$) at day 4 of infection was ascertained by ex vivo luciferase activity normalized for tissue protein amounts. (B) *Cxcl10* gene expression (qPCR) in the brain of WT and $IFN\beta$ and STING1 KO mice at day 4 of infection. (C) Representative flow cytometry dot plots showing the percentage of CD45^{high} cells within brain infiltrates of WT and STING1 KO mice. (D) Flow cytometry analysis of brain leukocytes isolated from noninfected or *Pba*-infected (day 6 PI) WT and STING1 KO mice. Extracellular staining against CD45 in combination with staining for TCRβ, CD8, and Mac-1 identified CD8⁺ T cells (CD45^{high} TCRβ⁺ CD8⁺), monocytes (CD45^{high} Mac-1⁺), and microglia (CD45^{int} Mac-1⁺). Activated CD8⁺ T cells were identified by extracellular expression of CD62L and CD44 and intracellular staining for Granzyme B and IFNγ. MHC I expression identified activated microglial cells. Experimental groups were compared using one-way ANOVA with Tukey's multiple comparisons test. Data points represent individual animals in A, B, and D. Data are analyzed by unpaired, two-tailed *t* test in A and B.

obtained from the serum of *P. berghei*-infected mice or from IE cell cultures can induce type I IFN signaling in primary cultures of BECs.

Nanoparticle tracking analysis of EPs collected from mouse serum showed significantly increased mean particle size in *Pba*-infected, CM-sick mice than in noninfected mice (Fig. 4A and S1

Appendix, Fig. S4A). Negative-stain transmission electron microscopy (TEM) (Fig. 4B) confirmed the presence of large particles with more than 200 nm in the serum of infected mice, while EPs isolated from noninfected animals were around 100 nm, the exosome size range (Fig. 4A). Moreover, the concentration of particles within the range of 100.5 to 265.5 nm increased

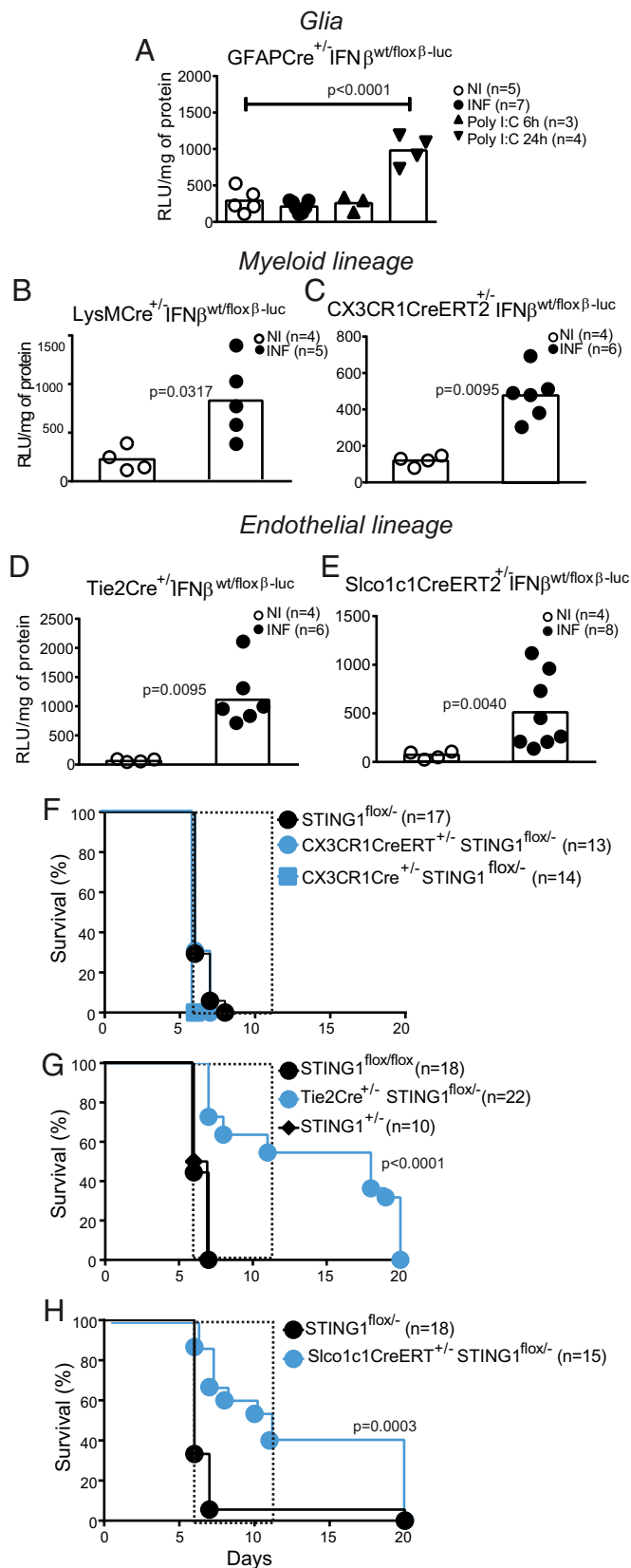


Fig. 3. STING1 expression on brain endothelial cells is a determinant of IFN β induction and CM lethality. *Ifn β 1* gene expression was ascertained by ex vivo luciferase activity in mice infected with *Pba* (day 6 PI) and noninfected mice carrying a IFN β -Luciferase reporter conditionally activated in cells expressing (A) GFAP (glial cells), (B) LysM (myeloid cells), (C) CX3CR1 (microglia cells), (D) Tie-2 (endothelial and hematopoietic cells), or (E) Slco1c1 (brain endothelial cells). I.p. injection of Poly I:C was used as positive response control of *Ifn β 1* gene induction. Results comprise two independent infection experiments and data are analyzed with unpaired, two-tailed

approximately threefold in the blood of infected mice compared to noninfected controls (*SI Appendix*, Fig. S4B). The particles isolated from blood of *Pba*-infected mice that differ from those found in noninfected mice were mostly from leukocyte (CD45⁺) and erythrocytic origin (TER119⁺) as revealed by antibody staining for cell-type surface markers (Fig. 4C).

In BEC cultures, particles isolated from the blood of mice with CM activated IFN β gene transcription (Fig. 4D) and protein expression (*SI Appendix*, Fig. S4C), but not those from noninfected mice. Similarly, EPs obtained from IE cultures activated *Ifn β 1* transcription measured by the luciferase activity in IFN β -reporter BECs (Fig. 4E). In contrast, neither erythrocytes from noninfected mice (NIEs) nor erythrocytes from *Pba*-infected mice (IEs) induced luciferase activity (Fig. 4E). To determine whether endosomal acidification was required for endothelial response, cells were pretreated with ammonium chloride, which elevates the intralysosomal pH (35). Remarkably, induction of IFN β in response to EPs was abolished in BECs preexposed to ammonium chloride (Fig. 4F). Furthermore, luciferase activity was lower in IFN β -reporter STING1 KO BECs stimulated with IE-derived EPs (Fig. 4G). This result indicates that *Sting1* deletion in BECs reduces induction of IFN β by IE-derived EPs. In sum, EPs derived from infected erythrocytes are processed in acidic compartments in BECs, activate STING1, and induce IFN β .

Particles Emanating from the Parasite's Digestive Vacuole Induce *Ifn β 1* and *Cxcl10* in Brain Endothelial Cells.

To identify bioactive factors associated with EPs that trigger type I IFN response in BECs, we established a protocol to fractionate bulk EPs obtained from *P. berghei* IE cultures on the basis of a combination of differential centrifugation, paramagnetic separation, and presence of host erythrocytic membrane (Fig. 5A). We found that compared to total EPs, the fraction (Fr1) pulled down at lower centrifugation ($5,630 \times g$) induced higher *Ifn β 1* transcription measured by luciferase activity (*SI Appendix*, Fig. S5A). Therefore, we further fractionated Fr1 using a magnetic LS column (Miltenyi Biotec) to separate a fraction enriched in particles containing iron and hemozoin (Fr2) from the flow through (Fr3) (Fig. 5A). To isolate particles with erythrocytic membrane (TER119⁺), Fr3 was incubated with biotinylated anti-TER119 antibody and streptavidin magnetic beads (Fig. 5A). The retained fraction in immunomagnetic separation originated the Fr4, and the flow through originated Fr5. Flow cytometry analysis (Fig. 5B and *SI Appendix*, Fig. S5B) showed that compared to Fr1, Fr2 and Fr5 are enriched in TER119⁻ particles. *Pba*-GFP parasites were used to generate IE cultures, thus, the GFP signal in Fr5 indicates the presence of parasite-derived material. TEM of fixed samples confirmed that Fr2 contained vesicles with hemozoin crystals likely derived from the parasite's digestive vacuoles (Fig. 5C). Among all fractions, the hemozoin-enriched Fr2, was the strongest inducer of luciferase activity in BECs. Compared to total EPs (2×10^6 EPs), a 10-fold lower amount (2×10^5 EPs) of Fr2 induced luciferase activity (Fig. 5D). In BECs, Fr2 was also a potent inducer of *Cxcl10* (Fig. 5E) and *Irf7* (*SI Appendix*, Fig. S5C) mRNA. Importantly, Fr2-induced expression of these genes was about

t test. Survival curves after *Plasmodium* infection in mice carrying conditional or induced STING deletion driven by (F) CX3CR1Cre and CX3CR1CreERT (monocytes/microglia), (G) Tie2Cre (endothelial cells), or (H) Slco1c1CreERT (brain endothelial). Results represent at least three independent infection experiments for each mouse strain. Survival curves were compared by a Gehan-Breslow-Wilcoxon test.

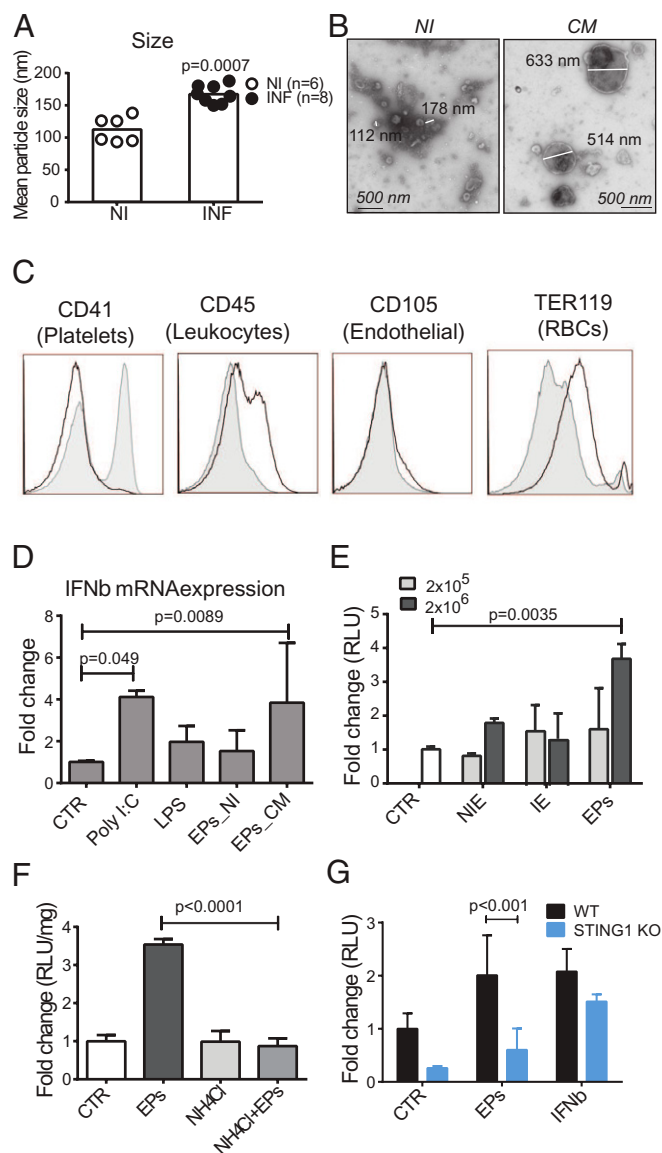


Fig. 4. EPs isolated from blood and IEs induce IFN β in brain endothelial cells after acidic processing and in a STING1-dependent manner. (A) NanoSight analysis of mean particle size after serum centrifugation (20,000 \times g) of symptomatic *Pba*-infected mice (day 6 PI) and noninfected control mice. Results represent two independent infection experiments. Noninfected mice were compared with *Pba*-infected mice by unpaired, two-tailed *t* test. (B) TEM image of negative stained EPs obtained from the serum of mice with CM or noninfected animals. (C) Representative flow cytometry histograms of serum EPs pooled from three to five animals and stained with the indicated cell lineage membrane markers. EPs were collected after 20,000 \times g centrifugation from noninfected (full histogram) and infected (empty histogram) mice. Data shown are representative of three independent experiments. (D) *Ifn β 1* RNA quantification in BECs stimulated with MPs isolated from the serum (600 μ L) of symptomatic *Pba*-infected mice (day 6 PI) (EPs-CM, *n* = 6 independent isolation experiments) and noninfected control mice (EPs-NI, *n* = 3 independent isolation experiments). Exposure to LPS (1 μ g/mL) and Poly I:C (5 μ g/mL) was used as positive response controls. (E) Measurement of luciferase activity in IFN β -reporter BECs exposed to two different doses (2×10^5 and 2×10^6) of erythrocytes isolated from the blood of noninfected (NIE) or *Pba*-infected mice (IE), or with EPs obtained from IE cultures centrifuged at 20,000 \times g. One representative experiment of two performed in duplicate or triplicate. (F) Activation of *Ifn β 1* gene expression measured by luciferase activity in IFN β -reporter BECs treated or not with NH₄Cl (20 mM) and then exposed to EPs collected from *Pba*-IE cell cultures. One representative experiment of three performed in triplicate is shown. (G) *Ifn β 1* gene expression measured by luciferase activity in IFN β -reporter WT or STING1 KO BECs stimulated with EPs. Results comprise data of two independent experiments done in triplicate. Treatments are compared between the two genotypes by two-way ANOVA using Tukey's multiple comparisons test. Data are presented as mean values \pm SD in D–G and analyzed by one-way ANOVA using Tukey's multiple comparisons test in D–F.

twofold lower in STING1 KO BECs than in WT BECs and was abolished in IFN β KO and in quadruple MyTrMaSt KO BECs (Fig. 5E and *SI Appendix*, Fig. S5C). Nevertheless, these KO BECs expressed *Cxcl10* and *Irf7* in response to direct stimulation with IFN β , which indicates that the IFN β –IFNAR axis was preserved (*SI Appendix*, Fig. S5D). Remarkably, neither exposure to IFN β nor to Fr2 affected the expression of adhesion molecules (VCAM-1, ICAM-1, PECAM-1, and E-Selectin) in WT and STING1 KO BECs, which were similarly induced upon exposure to TNF (*SI Appendix*, Fig. S5E).

These results indicate that Fr2, the IE-derived particle fraction containing digestive vacuole remnants, strongly induces a type I IFN response in BECs, which is at least partially dependent on STING1.

Labile Heme Originated by the Parasite Activates STING1 in Brain Endothelial Cells. We then addressed the role of hemozoin in STING1 activation by inhibiting the hemozoin synthesis pathway in IE cultures with chloroquine, an antimalarial drug described to increase the levels of labile heme in the parasite (15). Unexpectedly, EPs obtained from chloroquine-treated IE cell cultures induce stronger IFN β expression than EPs from untreated IEs (Fig. 6A). Both hemozoin and labile heme can activate PRRs and contribute to an inflammatory storm and BBB dysfunction in CM (14, 16, 17). We stimulated BECs directly with different amounts of heme and hemozoin. While hemozoin was unable to stimulate BECs, 20 μ M of heme induced significant luciferase activity in WT but not in STING1 KO IFN β -reporter BECs (Fig. 6B and *SI Appendix*, Fig. S5F). Moreover, heme induced *Cxcl10* gene expression in WT BECs, as previously described (36), but not in STING1 KO BECs (Fig. 6C).

Following these results, we tested a putative interaction of heme with STING1 by performing docking calculations. GOLD software was used to dock heme into the structure of STING1 and search for the optimal pose (orientation, conformation, and binding energy) between them. We found that the heme is positioned within the STING1 binding site for its ligand *c*-di-GMP, mostly overlapping with it (Fig. 6D and *SI Appendix*, Fig. S5G). This shows that heme can position itself in the pocket in a propitious way for interaction with STING1. Although well positioned, heme has less affinity to STING1 than *c*-di-GMP (ChemPLP score of 61 for heme compared to 104 for *c*-di-GMP). We next tested the ability of STING1 to bind heme by examining the peroxidase-like activity and migration shift of recombinant human STING1 upon incubation with heme. We detected peroxidase activity of STING1–heme complexes at the molar ratio of 1:150, while protein shift was detected at a molar ratio of 1:60 (Fig. 6E), values that are similar to those reported for other heme-binding proteins in this assay (37).

Taken together, the results indicate that heme-containing EPs derived from IEs are able to induce type I IFN responses in BECs in a STING1-dependent manner, possibly involving direct heme binding to STING1.

Discussion

We identified STING1 activation in brain endothelial cells as a molecular pathway that mediates neuroinflammation and brain pathology underlying the pathogenesis of CM. We demonstrated that, early in infection, the brain endothelium uses STING1 to sense *Plasmodium* blood-stage infection and initiate a type I IFN response through activation of *Ifn β 1* and

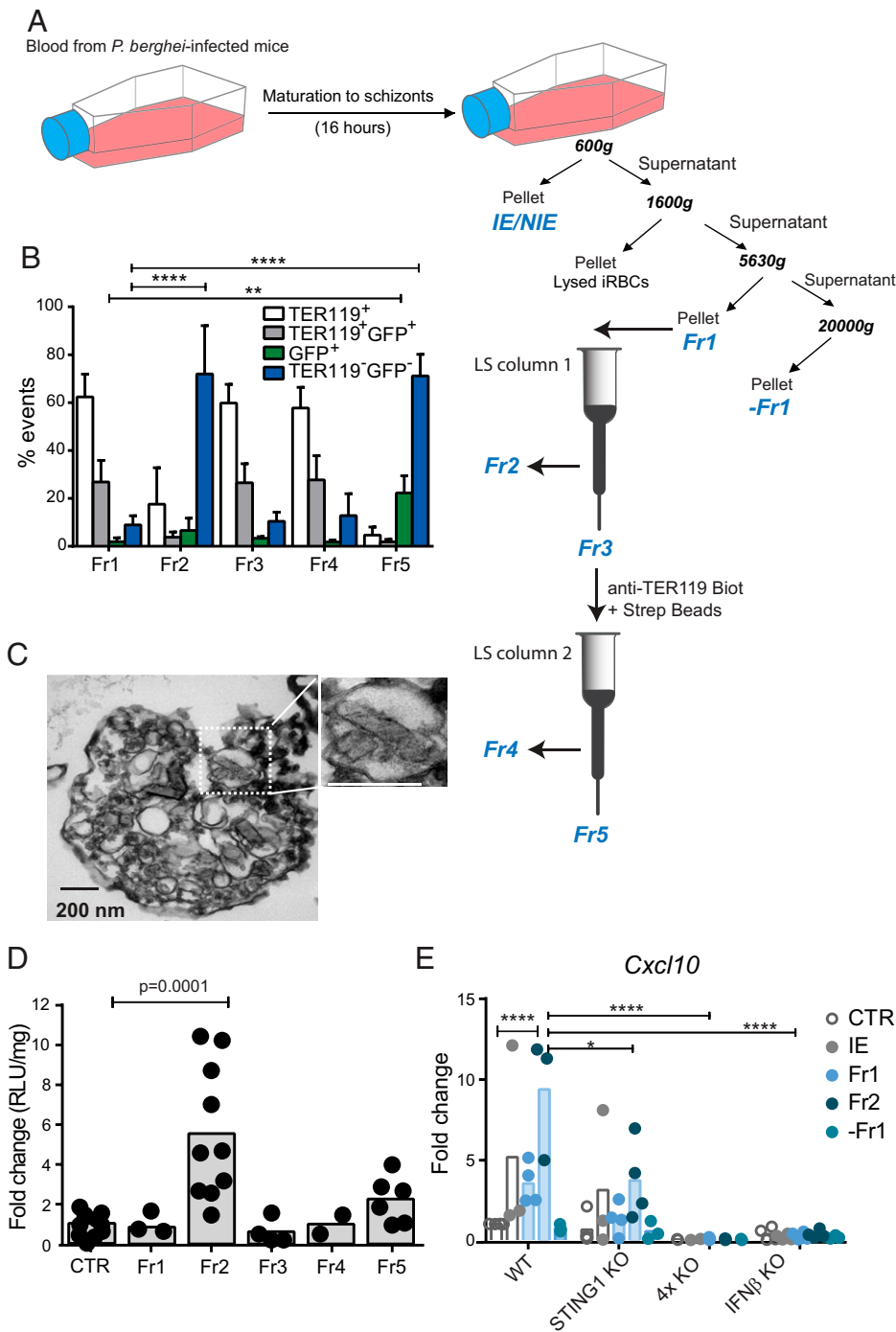


Fig. 5. Particles derived from the parasite's digestive-vacuole activate type I IFN response in brain endothelial cells. (A) Experimental workflow for EP fractionation from *Pba*-IE cultures combining multistep centrifugation with magnetic and immunomagnetic separation to obtain five fractions (Fr1 to Fr5). Fr2 is isolated by magnetic field capture of iron-enriched EPs. Fr4 is obtained by immunoseparation of EPs expressing the erythrocyte surface marker Ter119. (B) Flow cytometry analysis of EPs staining for TER119 and/or GFP⁺. Data comprising four independent experiments were compared to Fr1 by two-way ANOVA, Dunnett's multiple comparisons test. *****P* < 0.0001, ***P* < 0.01. (C) TEM imaging of Fr2 (fixed sample) showing membrane structures surrounding hemazoin crystals. (D) Measurement of luciferase activity in IFNβ-reporter BECs stimulated with each one of the five different EP fractions; at 2 × 10⁵ EPs/fraction. Data comprise 2 (Fr4), 4 (Fr1 and Fr3), 6 (Fr5), and 10 (Fr2) independent isolation experiments and each spot represents a cell culture well. One-way ANOVA, Tukey's multiple comparisons test. (E) *Cxcl10* gene expression in BECs stimulated with blood of *Pba*-infected mice containing 2 × 10⁵ IEs and with 2 × 10⁵ EPs of different fractions. Data comprise three to four experiments of different BEC and EP isolations and are compared between genotypes by two-way ANOVA using Tukey's multiple comparisons test, **P* < 0.05, *****P* < 0.0001. Each spot represents a cell culture well.

Cxcl10 gene transcription. This is associated with leukocyte recruitment and subsequent loss of BBB function, a hallmark of CM. We found that extracellular particles derived from IEs, containing hemazoin and enriched for labile heme, trigger STING1-dependent IFNβ responses in brain endothelial cells (Fig. 6F).

Our study identifies IFNβ as a critical trigger of IFNAR signaling and a determinant of BBB disruption and lethality in CM. Whole and cell-specific IFNβ-reporter mice enabled us to identify BECs, as well as brain monocytes/microglia, as main producers of IFNβ, and STING1 as the key PRR upstream of IFNβ induction. STING1—a main activator of *Irf1* transcription—also controlled

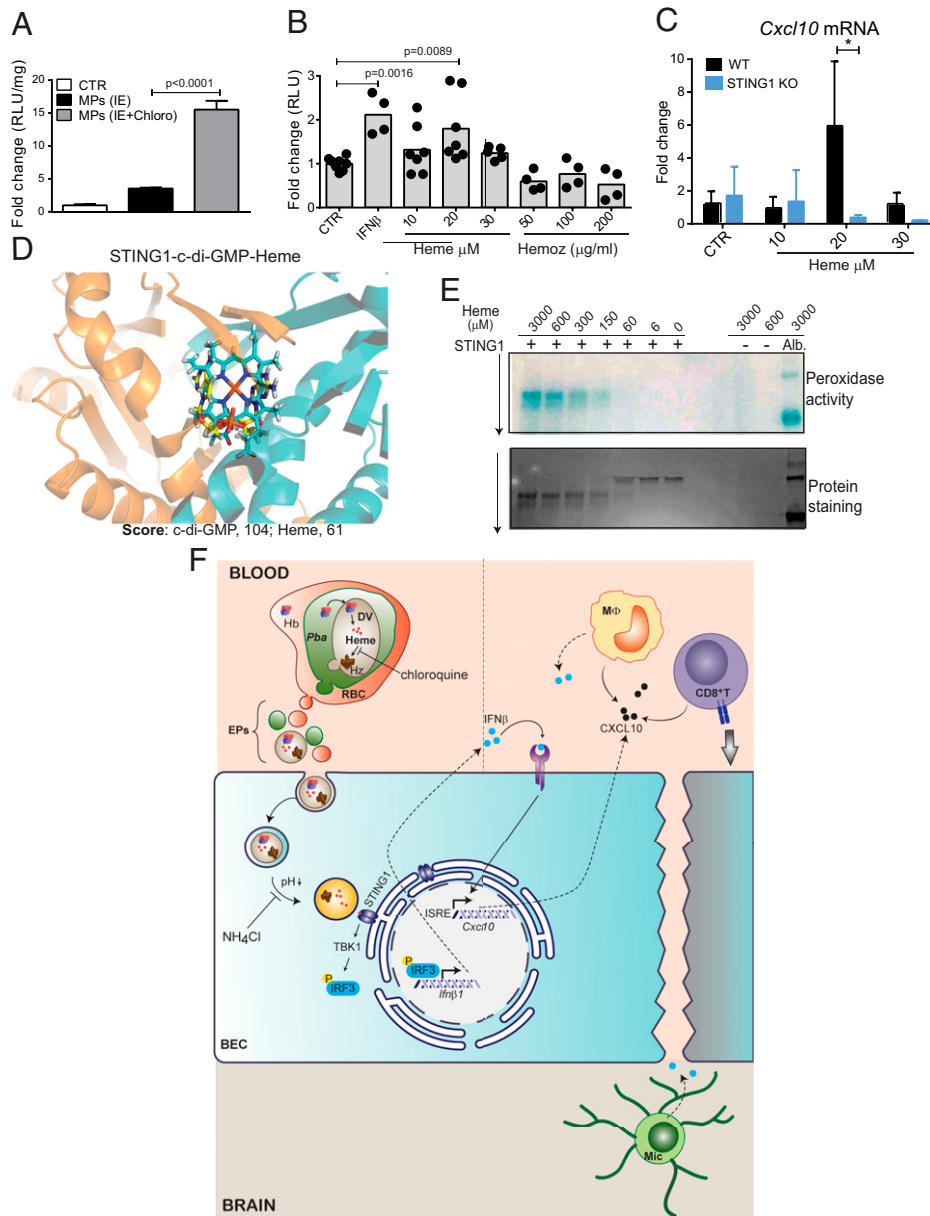


Fig. 6. Heme sequestered by the parasite induce *Ifnβ1* and *Cxcl10* gene expression in BECs through STING1 activation. (A) Luciferase activity in IFNβ-reporter BECs exposed to 2×10^6 EPs from *Pba* IE cultured in the presence or absence of chloroquine (8 μM). One representative experiment of two performed in triplicate is shown. (B) Luciferase activity in IFNβ-reporter BECs stimulated with hemin or hemozoin at the indicated concentrations or with IFNβ (1,000 U/mL). Data comprise two to three independent experiments and each point represents a cell culture well. (C) *Cxcl10* gene expression in WT or STING1 KO BECs stimulated with different concentrations of hemin for 20 h. Data comprise two independent experiments. Comparison between genotypes was performed by two-way ANOVA, Tukey's multiple comparisons test, * $P < 0.05$. (D) STING1-heme molecular docking results. Closeup view of STING1 pocket with superposition of best-scoring docked pose of c-di-GMP and heme. c-di-GMP and heme are colored in yellow and cyan sticks, respectively. Molecular docking was performed using GOLD software and ChemPLP as scoring function. (E) Detection of peroxidase activity and migration shift assay of STING1 (1 μM) incubated with increasing doses of heme. Albumin (5 μM) incubated with heme was used as positive control for peroxidase activity and heme alone was used as negative control. (F) Schematic model of STING1 activation in brain endothelium by parasite-derived heme-containing particles and its contribution to the pathogenesis of cerebral malaria. Hb, hemoglobin; DV, digestive vacuole; RBC, red blood cell; MΦ, monocyte; Mic., microglia; TBK1, TANK binding kinase 1; IRF3, interferon regulatory factor 3; ISRE, interferon-sensitive response element. Data are presented as mean values \pm SD in A–C and analyzed by one-way ANOVA using Tukey's multiple comparisons test in A and B.

early *Cxcl10* gene induction in the brain of *Pba*-infected mice. CXCL10 is known to promote chemotaxis of CXCR3 expressing CD8⁺ T cells to the central nervous system during *Toxoplasma* infection (28) and has been strongly linked to CM severity both in humans (38, 39) and in rodents (27). We observed that both IFNβ KO and STING1 KO have lower numbers of CD8⁺ T cells and monocytes in the brain infiltrates. Thus, our data support a role for CXCL10 in inducing chemotactic leukocyte migration into the brain. It remains to be determined whether

parasite-specific CD8⁺ T cells in STING1 or IFNβ KO mice are less prone to CXCL10–CXCR3 chemotactic migration.

Here, we demonstrated that activation of STING1 in BECs promotes CM pathology. Infected mice whose brain endothelial/ependymal cells are made deficient in STING1 (*Slco1c1*-CreERT STING1 floxed mice) displayed milder neurological deficits and increased survival. Several studies reported that plasmodial DNA activates STING1 in innate immune cells such as monocytes and macrophages (12, 19, 20). However, we

found that specific *Irfβ1* or *Sting1* deletion in myeloid and microglia cells did not affect CM development in mice. Instead, our data indicate that BECs are the main cell drivers of the STING1–IFNβ axis in the brain during CM. Nevertheless, STING1 or IFNβ ablation does not completely prevent CM, suggesting CD8⁺ T cell activation in the spleen is operating and recruitment of activated leukocytes, albeit at lower levels, occurs through alternative mechanisms.

STING1 is localized in the endoplasmic reticulum (ER) and does not bind DNA directly, but interacts with cyclic dinucleotides, namely cGAMP. cGAMP is produced by cyclic-GMP-AMP synthase (cGAS) upon dsDNA sensing in the cytosol. After translocation into the Golgi apparatus, STING1 and TBK1 phosphorylate IRF3 that promotes transcription of type I IFN genes (40). Interestingly, a population of exosomes isolated from *P. falciparum* (*Pf*) IE cultures at the ring stage, could transfer *Pf* DNA to peripheral blood mononuclear cells and activate the cGAS–STING1 pathway with consequent induction of *Irfβ1/α* gene expression (19). Our study further highlights the likely important role for IE-derived particles in the activation of innate immune mechanisms during malaria. We found that IE-derived particles larger than exosomes and enriched in vesicles containing hemozoin are able to activate *Irfβ* and *Cxcl10* transcription in BECs. This activation depends on intracellular organelle acidification, suggesting a requirement for endosome maturation and/or acidic hydrolase activity (35). IE-derived particles containing hemozoin could represent digestive vacuoles that accumulate heme and/or hemoglobin. In line with these findings, it has been previously shown that digestive vacuoles but not merozoites or isolated hemozoin activate the complement in vivo (41), which could facilitate the uptake of these vesicles by the brain endothelium. Although plasmodial DNA bound to hemozoin has been shown to activate cyclic GMP-AMP (cGAS) upstream of STING1 in macrophages (12), hemozoin itself does not seem to be required for STING1 activation in BECs. In fact, exposure of IEs to chloroquine, which reduces hemozoin and increases labile heme bioavailability, enhances IFNβ in BECs. This prompted us to hypothesize that heme could be involved in STING1 activation mediated by IE-derived EPs. Indeed, we observed STING1-dependent up-regulation of *Irfβ* and *Cxcl10* in the presence of labile heme at concentrations within the ranges found in the plasma of children with CM (42) and known to activate *Cxcl10* transcription in endothelial cells (36). Recently, hemolysis in sickle cell disease and injection of hemin in mice were shown to activate and recruit monocytes to the liver through activation of type I IFN signaling and independently of TLR4 (43). Our docking experiments and protein binding assay indicate that heme can bind STING1 in vitro. However, further evidence of direct binding of heme to STING1 in the ER is required to clarify whether heme is a direct or indirect activator of STING1 in BECs. Interestingly, late endosomes tightly contact with the ER (44), indicating that heme–STING1 interaction may occur during the association between acidified mature endosomes containing heme and the ER (Fig. 6F).

Overall, we demonstrate that STING1 in the brain endothelium senses molecular by-products of erythrocyte infection by *Plasmodium*, such as labile heme, initiating a type I IFN response mediated by IFNβ with induction of CXCL10 in early phases of infection. This, in turn, triggers a cascade of events that promote brain inflammation, including leukocyte recruitment, and may also affect neuronal responses. This study suggests that type I IFN–targeted strategies may minimize brain immunopathology, thus preventing fatal CM and subsequent neurological sequels in survivors.

Materials and Methods

Detailed descriptions for all procedures are available in *SI Appendix*.

Mice and Treatments. All procedures involving laboratory mice were in accordance with national (Portaria 1005/92) and European regulations (European Directive 86/609/CEE) on animal experimentation and approved by the Instituto Gulbenkian de Ciência (IGC) Ethics Committee and the Direção-Geral de Alimentação e Veterinária, the national authority for animal welfare.

Mice strains used and generated in this study (*SI Appendix, Table S1*) were C57BL/6 genetic background and were housed and bred in the facilities of IGC. Wild-type, deleted, and floxed alleles of *Irfβ1* and *Sting1* were identified in experimental animals by genotyping using a three-primer strategy (*SI Appendix, Table S2*). For induction of *Sting1* deletion, 4- to 6-wk-old male and female mice were treated with tamoxifen (2 mg/10 g body weight) in corn oil administered by gavage every other day, totaling five doses. Mice were allowed to recover from tamoxifen treatment for 4 wk.

For in vivo labeling of proliferating cells, mice received four intraperitoneal (i.p.) injections of BrdU (50 mg/kg,) every 2 h.

Parasites and Infection. Mice were infected with 10⁶ IEs with the following parasite strains: *P. berghei* ANKA (*Pba*), *Pba*-GFP (45), or *Pba* line expressing luciferase (clone 676m1d1) (46) to induce CM or with *Pb* NK65 (47), a strain that proliferates in mice but does not induce neurological signs of CM. Frozen IE stocks were expanded in C57BL/6 mice prior to infection. Parasitemia in mice infected with non-GFP parasites (*Pba* and *Pb* NK65) and GFP-*Pba* was determined by flow cytometry.

Evaluation of CM.

Neurological score. Wild-type mice developed severe signs of CM such as head deviation, paralysis, and convulsions at days 6 to 7PI and died within 4 to 6 h of severe disease development. Mice resistant to CM died around day 20 with hyperparasitemia (~60%) without signs of severe neurological dysfunction.

Disease severity was evaluated in mice before and after infection following an adapted health score for CM (48).

Blood-brain barrier integrity assay. At day 6 PI, when C57BL/6J WT mice show signs of CM, the different mouse groups were killed 1 h after retroorbital injection of 100 μL of 2% EB dye (Sigma) and were perfused intracardially with 15 mL of phosphate buffer saline (PBS). Brains were dissected, weighed, and pictured. EB retained in the brain tissue was extracted and measured by spectrophotometry at 620 and 740 nm (Thermo Scientific Multiskan GO Microplate Spectrophotometer). Amounts of EB were calculated using an EB standard and expressed as milligrams of EB per gram of brain tissue.

Immune cells analysis. Spleen (day 5 PI) and brain (day 6 PI) single-cell suspensions of infected and noninfected C57BL/6J and KO mice were immunostained for T cell and monocyte/macrophage activation cell surface markers (*SI Appendix, Table S3*). Brain single-cell suspensions were prepared as described before (25). Data were analyzed with FlowJo v10 software and cell types identified according to the gate strategy (*SI Appendix, Fig. S6*).

Isolation of EPs. All the solutions were filtered (0.22 μm) before use. Blood EPs were obtained from mouse blood collected by cardiac puncture. Plasma was prepared by two successive centrifugations at 1,500 × *g* for 15 min at 4 °C. Harvested plasma was further centrifuged at 20,000 × *g* for 25 min and the pellet containing EPs was resuspended in 0.2% bovine serum albumin (BSA) in PBS (49).

IE-derived EPs were prepared from the supernatant of IE cultures. EPs were isolated adapting a previously described procedure (34) (Fig. 5A). Briefly, the cell suspension was first centrifuged at 600 × *g* to remove IEs and non-IEs and then centrifuged at 1,600 × *g* for 15 min to remove cell debris. The supernatant of this centrifugation was then sequentially centrifuged at 5,630 × *g* and 20,000 × *g* for 20 min (total EPs). The pellet resulting from centrifugation at 5,630 × *g* was designated fraction 1 (Fr1) and the supernatant was further centrifuged at 20,000 × *g* producing a pellet, “-Fr1.” Fr1 was resuspended in PBS and passed through a LS magnetic exclusion column according to the manufacturer’s instructions (MACS Milteny Biotec). Particles retained in this column were designated Fr2. The flow through (Fr3) was centrifuged at 10,000 × *g* for 10 min and the obtained pellet incubated with biotinylated anti-mouse TER119 antibody (1 μg/mL) (Invitrogen). The pellet was then washed twice and resuspended in 80 μL of

labeling buffer (PBS, 2 mM ethylenediaminetetraacetic acid, EDTA) containing 20 μ L of Anti-Biotin MicroBeads (Milteny Biotec). After incubation for 15 min at 4 °C and washing, the pellet was resuspended in separation buffer (0.5% BSA, 2 mM EDTA in PBS) followed by magnetic separation through a second LS column. Particles retained in this column and flow through were designated Fr4 and Fr5, respectively.

Characterization of extracellular particles (EPs).

NanoSight. Blood-derived EPs were analyzed for particle concentration and size distribution by the NS300 Nanoparticle Tracking Analysis system with a red laser (638 nm) (NanoSight-Malvern Panalytical).

Flow cytometry. Blood MPs or IE-derived EPs were preincubated with Fc block and then stained with phycoerythrin (PE)-conjugated anti-mouse Ter119, CD41, CD45, and CD105 antibodies (1:100) (Life Technologies). Samples were acquired with flow cytometer LSRFortessa (BD Biosciences, run with FACSDiVa software version 6.2) using side scatter of blue violet laser (SSC-BV) and the photomultiplier tube option for the forward scatter channel (FSC-PMT) to detect small particles. Total EP numbers were calculated using 5,000 counting beads (10 μ m) in each sample.

Transmission electron microscopy. EPs were processed for negative staining or fixed with 2% formaldehyde and 2.5% glutaraldehyde in 0.1 M phosphate buffer (PB) overnight at 4 °C.

Electron microscopy images were acquired on a FEI Tecnai G2 Spirit BioTWIN transmission electron microscope operating at 120 keV and equipped with an Olympus-SIS Veleta charge-coupled device (CCD) camera.

Brain Endothelial Cell Cultures. Mouse brains were removed from the skull and kept in a Petri dish with Hank's Balanced Salt Solution (HBSS) medium (Bio-west) on ice. The brains were transferred to a freezer block covered with gauze and the meninges removed by rolling a cotton swab over each brain. Brain blood vessels were then isolated adapting a previously described procedure (50). When cultures reached 50 to 80% confluence (~14 d, 95% of the cells are CD31⁺ by flow cytometry analysis), cells were exposed for 18 to 20 h to different amounts (2×10^5 to 2×10^6) of IEs and NIEs, EP fractions (total EPs, -Fr1 and Fr1 to Fr5), EPs (present in 600 μ L of serum), or different activators of IFN β signaling (IFN β , 1,000 U/mL; lipopolysaccharide (LPS), 1 μ g/mL; Poly I:C, 1 to 5 μ g/mL). To inhibit endosome acidification, BECs were preincubated for 20 min with 20 mM of NH₄Cl before adding the stimuli.

Heme was added as ferric chloride heme (hemin, Sigma) to BECs at a final concentration range of 10 to 30 μ M. A freshly prepared stock solution was obtained by dissolving hemin in NaOH 0.1 M for 1 h at 37 °C and then adding 1 M Tris, pH 7.5 to a final concentration of 0.1 M. HCl was added to the solution to bring the pH back to 7.5.

Molecular Docking. STING1-c-di-GMP crystal structure (PDB ID: 6S26) was retrieved from the Protein Data Bank (PDB). C-di-GMP was then removed and redocked into the corresponding STING1 crystal structure. Upon self-docking successfully validating the developed protocol, molecular docking of heme was performed, 500 GA runs. Heme followed the same ligand preparation procedure as c-di-GMP.

Peroxidase Activity and Gel Migration Shift Assay. Recombinant human STING1 protein (Gentaur) (0.3 μ g, 1 μ M) in 20 mM Tris-HCl, 0.15 M NaCl, pH = 8.0 (Tris buffer) was incubated for 15 min at room temperature with 3,000, 600, 300, 150, 60, and 6 μ M of heme. After adding Tris sample buffer (pH = 6.8) for native polyacrylamide gel electrophoresis (PAGE) (no sodium dodecyl sulfate, SDS, or reducing agents), the samples were loaded on 12%

Criterion TGX Stain-Free precast gels for PAGE (Bio-Rad). Heme-STING1 complexes were separated by gel electrophoresis in nondenaturing running buffer. Peroxidase-like activity of heme bound to STING1 was detected on the gel after incubation with a TMB Substrate Reagent Set (BD Biosciences). STING1 without incubation with heme and heme alone were used as negative controls for peroxidase-like activity. Serum bovine albumin (3.3 μ g, 5 μ M) incubated with 600 μ M of heme was used as a positive control (51).

Gene Expression. RNA was prepared from total mouse brains of mice and from BECs using TRIzol and Cells-to-CT kit (Thermo Fisher Scientific), respectively. *Irf1*, *Cxcl10*, *Irf7*, *Irf1*, *Irfit1*, *Vcam1*, *Icam1*, *Pecam1*, and *Sele* mRNA were quantified using Mm00439552_s1, Mm00445235_m1, Mm00516788_m1, Mm01288580_m1 and Mm00515153_m1, Mm01320970_m1, Mm00516023_m1, Mm01242576_m1, and Mm00441278_m1 TaqMan Gene Expression Assays from ABI, respectively. cDNA specific to *P. berghei* 18S rRNA was amplified with TaqMan-specific primers: forward, 5'-CCG ATA ACG AAC GAG ATC TTA ACC T-3'; reverse, 5'-CGT CAA AAC CAA TCT CCC AAT AAA GG-3'; probe, 5'-ACT CGC CGC TAA TTA G-3' (FAM/MGB).

IFN β -Luciferase Reporter Assay. Tissues were lysed in Glo Lysis Buffer (Promega) followed by centrifugation at 20,000 $\times g$ for 20 min. BECs were gently washed with PBS before lysis. A total of 50 μ L of tissue or cell lysates were mixed with 50 μ L of Bright-Glo Luciferase Assay System (Promega) in a 96-well luminometer plate. The luminescence was immediately measured with GloMax Explorer (Promega) (excitation, 405 nm; emission, 500 to 550 nm; integration time, 5). Protein was quantified by Bradford Assay (Bio-Rad) and luciferase activity expressed as relative light unit (RLU) per milligram of protein.

Statistical Analysis. Statistical analysis was performed using Prism v6.01 software (GraphPad Software, Inc.). Comparisons between treated and nontreated conditions used two-tailed unpaired *t* test, comparisons between multiple groups used one-way analysis of variance (ANOVA), and comparisons between treated cells of different genotypes used two-way ANOVA as indicated in the figure legends. Bars in figures represent the mean (\pm SD) and each symbol represents one mouse or well, as indicated in the figures. Sample size and number of the independent experiments performed can be found in the figures and figure legends.

Data, Materials, and Software Availability. All study data are included in the main text and/or *SI Appendix*.

ACKNOWLEDGMENTS. We gratefully acknowledge the Electron Microscopy Unit at IGC, in particular Ana Laura Sousa for technical support. We thank M. Soares and S. Gomes for discussions and critical reading of the manuscript. This work was supported by ERA-NET NEURON and developed with the support from the research infrastructure CONGENTO, co-financed by FCT (Portugal) and Lisboa2020, under the project LISBOA-01-0145-FEDER-022170.

Author affiliations: ^aInstituto Gulbenkian de Ciéncia, 2780-156 Oeiras, Portugal; ^bCentro de Investigaço Interdisciplinar em Sanidade Animal, Faculdade de Medicina Veterinria, Universidade de Lisboa, 1300-477 Lisbon, Portugal; ^cInstitute for Experimental Infection Research, TWINCORE, Centre for Experimental and Clinical Infection Research, Helmholtz Centre for Infection Research and the Hannover Medical School, 30625 Hannover, Germany; ^dInstitute of Neuropathology, Medical Faculty, University of Freiburg, D-79106 Freiburg, Germany; ^eResearch Institute for Medicines, Faculty of Pharmacy, Universidade de Lisboa, 1649-003 Lisbon, Portugal; and ^fSystems Oncology Group, Champalimaud Research, Champalimaud Centre for the Unknown, 1400-038 Lisbon, Portugal

1. R. Idro, K. Marsh, C. C. John, C. R. J. Newton, Cerebral malaria: Mechanisms of brain injury and strategies for improved neurocognitive outcome. *Pediatr. Res.* **68**, 267-274 (2010).
2. K. B. Seydel *et al.*, Brain swelling and death in children with cerebral malaria. *N. Engl. J. Med.* **372**, 1126-1137 (2015).
3. J. Dunst, F. Kamena, K. Matuschewski, Cytokines and chemokines in cerebral malaria pathogenesis. *Front. Cell. Infect. Microbiol.* **7**, 324 (2017).
4. U. Frevert, A. Nacer, Fatal cerebral malaria: A venous efflux problem. *Front. Cell. Infect. Microbiol.* **4**, 155 (2014).
5. I. Sebina, A. Haque, Effects of type I interferons in malaria. *Immunology* **155**, 176-185 (2018).
6. M. Krupka *et al.*, Mild Plasmodium falciparum malaria following an episode of severe malaria is associated with induction of the interferon pathway in Malawian children. *Infect. Immun.* **80**, 1150-1155 (2012).
7. C. M. Feintuch *et al.*, Type I interferon receptor variants in gene regulatory regions are associated with susceptibility to Cerebral Malaria in Malawi. *Am. J. Trop. Med. Hyg.* **98**, 1692-1698 (2018).
8. A. M. Vigrio *et al.*, Recombinant human IFN- α inhibits cerebral malaria and reduces parasite burden in mice. *J. Immunol.* **178**, 6416-6425 (2007).
9. A. Hassan *et al.*, A virus hosted in malaria-infected blood protects against T cell-mediated inflammatory diseases by impairing DC function in a type I IFN-dependent manner. *MBio* **11** (2020), 7, 11(2):e03394-19. doi: 10.1128/mBio.03394-19.
10. E. A. Ball *et al.*, IFNAR1 controls progression to cerebral malaria in children and CD8+ T cell brain pathology in Plasmodium berghei-infected mice. *J. Immunol.* **190**, 5118-5127 (2013).
11. C. L. Edwards *et al.*, Spatiotemporal requirements for IRF7 in mediating type I IFN-dependent susceptibility to blood-stage Plasmodium infection. *Eur. J. Immunol.* **45**, 130-141 (2015).
12. S. Sharma *et al.*, Innate immune recognition of an AT-rich stem-loop DNA motif in the Plasmodium falciparum genome. *Immunity* **35**, 194-207 (2011).
13. S. Torre *et al.*, USP15 regulates type I interferon response and is required for pathogenesis of neuroinflammation. *Nat. Immunol.* **18**, 54-63 (2017).
14. R. T. Gazzinelli, P. Kalantari, K. A. Fitzgerald, D. T. Golenbock, Innate sensing of malaria parasites. *Nat. Rev. Immunol.* **14**, 744-757 (2014).

15. S. E. Francis, D. J. Sullivan Jr., D. E. Goldberg, Hemoglobin metabolism in the malaria parasite *Plasmodium falciparum*. *Annu. Rev. Microbiol.* **51**, 97–123 (1997).
16. M. P. Soares, M. T. Bozza, Red alert: Labile heme is an alarmin. *Curr. Opin. Immunol.* **38**, 94–100 (2016).
17. A. Pamplona *et al.*, Heme oxygenase-1 and carbon monoxide suppress the pathogenesis of experimental cerebral malaria. *Nat. Med.* **13**, 703–710 (2007).
18. A. Ferreira *et al.*, Sickle hemoglobin confers tolerance to *Plasmodium* infection. *Cell* **145**, 398–409 (2011).
19. X. Sisquella *et al.*, Malaria parasite DNA-harboring vesicles activate cytosolic immune sensors. *Nat. Commun.* **8**, 1985 (2017).
20. C. Gallego-Marin *et al.*, Cyclic GMP-AMP synthase is the cytosolic sensor of *Plasmodium falciparum* genomic DNA and activates type I IFN in malaria. *J. Immunol.* **200**, 768–774 (2018).
21. S. W. Howland, C. M. Poh, L. Rénia, Activated brain endothelial cells cross-present malaria antigen. *PLoS Pathog.* **11**, e1004963 (2015).
22. R. Jambou *et al.*, *Plasmodium falciparum* adhesion on human brain microvascular endothelial cells involves transmigration-like cup formation and induces opening of intercellular junctions. *PLoS Pathog.* **6**, e1001021 (2010).
23. F. E. Lovegrove *et al.*, Expression microarray analysis implicates apoptosis and interferon-responsive mechanisms in susceptibility to experimental cerebral malaria. *Am. J. Pathol.* **171**, 1894–1903 (2007).
24. S. Lienenklaus *et al.*, Novel reporter mouse reveals constitutive and inflammatory expression of IFN- β in vivo. *J. Immunol.* **183**, 3229–3236 (2009).
25. T. F. Pais, S. Chatterjee, Brain macrophage activation in murine cerebral malaria precedes accumulation of leukocytes and CD8+ T cell proliferation. *J. Neuroimmunol.* **163**, 73–83 (2005).
26. E. W. Sorensen *et al.*, CXCL10 stabilizes T cell-brain endothelial cell adhesion leading to the induction of cerebral malaria. *JCI Insight* **3**, e98911 (2018).
27. G. S. V. Campanella *et al.*, Chemokine receptor CXCR3 and its ligands CXCL9 and CXCL10 are required for the development of murine cerebral malaria. *Proc. Natl. Acad. Sci. U.S.A.* **105**, 4814–4819 (2008).
28. T. H. Harris *et al.*, Generalized Lévy walks and the role of chemokines in migration of effector CD8+ T cells. *Nature* **486**, 545–548 (2012).
29. E. Solodova, J. Jablonska, S. Weiss, S. Lienenklaus, Production of IFN- β during *Listeria monocytogenes* infection is restricted to monocyte/macrophage lineage. *PLoS One* **6**, e18543 (2011).
30. S. Yona *et al.*, Fate mapping reveals origins and dynamics of monocytes and tissue macrophages under homeostasis. *Immunity* **38**, 79–91 (2013).
31. D. A. Ridder *et al.*, TAK1 in brain endothelial cells mediates fever and lethargy. *J. Exp. Med.* **208**, 2615–2623 (2011).
32. J. B. Pankoui Mfonkeu *et al.*, Elevated cell-specific microparticles are a biological marker for cerebral dysfunctions in human severe malaria. *PLoS One* **5**, e13415 (2010).
33. F. El-Assaad, J. Wheway, N. H. Hunt, G. E. R. Grau, V. Combes, Production, fate and pathogenicity of plasma microparticles in murine cerebral malaria. *PLoS Pathog.* **10**, e1003839 (2014).
34. P. Y. Mantel *et al.*, Malaria-infected erythrocyte-derived microvesicles mediate cellular communication within the parasite population and with the host immune system. *Cell Host Microbe* **13**, 521–534 (2013).
35. I. Mellman, R. Fuchs, A. Helenius, Acidification of the endocytic and exocytic pathways. *Annu. Rev. Biochem.* **55**, 663–700 (1986).
36. C. M. Dickinson-Copeland *et al.*, Heme-mediated induction of CXCL10 and depletion of CD34+ progenitor cells is toll-like receptor 4 dependent. *PLoS One* **10**, e0142328 (2015).
37. E. Karnaukhova *et al.*, Characterization of heme binding to recombinant α 1-microglobulin. *Front. Physiol.* **5**, 465 (2014).
38. H. B. Armah *et al.*, Cerebrospinal fluid and serum biomarkers of cerebral malaria mortality in Ghanaian children. *Malar. J.* **6**, 147 (2007).
39. V. Jain *et al.*, Plasma IP-10, apoptotic and angiogenic factors associated with fatal cerebral malaria in India. *Malar. J.* **7**, 83 (2008).
40. D. Wan, W. Jiang, J. Hao, Research advances in how the cGAS-STING pathway controls the cellular inflammatory response. *Front. Immunol.* **11**, 615 (2020).
41. P. Dasari *et al.*, Digestive vacuole of *Plasmodium falciparum* released during erythrocyte rupture dually activates complement and coagulation. *Blood* **119**, 4301–4310 (2012).
42. R. E. Elphinstone *et al.*, Dysregulation of the haem-haemopexin axis is associated with severe malaria in a case-control study of Ugandan children. *Malar. J.* **14**, 511 (2015).
43. Y. Liu *et al.*, Type I interferon is induced by hemolysis and drives antibody-mediated erythrophagocytosis in sickle cell disease. *Blood* **138**, 1162–1171 (2021).
44. J. R. Friedman, J. R. Dibenedetto, M. West, A. A. Rowland, G. K. Voeltz, Endoplasmic reticulum-endosome contact increases as endosomes traffic and mature. *Mol. Biol. Cell* **24**, 1030–1040 (2013).
45. B. Franke-Fayard *et al.*, A *Plasmodium berghei* reference line that constitutively expresses GFP at a high level throughout the complete life cycle. *Mol. Biochem. Parasitol.* **137**, 23–33 (2004).
46. C. J. Janse, J. Ramesar, A. P. Waters, High-efficiency transfection and drug selection of genetically transformed blood stages of the rodent malaria parasite *Plasmodium berghei*. *Nat. Protoc.* **1**, 346–356 (2006).
47. L. Vandermosten *et al.*, Experimental malaria-associated acute respiratory distress syndrome is dependent on the parasite-host combination and coincides with normocyte invasion. *Malar. J.* **17**, 102 (2018).
48. R. W. Carroll *et al.*, A rapid murine coma and behavior scale for quantitative assessment of murine cerebral malaria. *PLoS One* **5**, 1–12 (2010).
49. S. Dinkla, R. Brock, I. Joosten, G. J. Bosman, Gateway to understanding microparticles: Standardized isolation and identification of plasma membrane-derived vesicles. *Nanomedicine (Lond.)* **8**, 1657–1668 (2013).
50. S. W. Howland, S. Y. Gun, C. Claser, C. M. Poh, L. Rénia, Measuring antigen presentation in mouse brain endothelial cells ex vivo and in vitro. *Nat. Protoc.* **10**, 2016–2026 (2015).
51. F. A. Englert *et al.*, Labile heme impairs hepatic microcirculation and promotes hepatic injury. *Arch. Biochem. Biophys.* **672**, 108075 (2019).